Fermi surface topology and anisotropic superconducting gap in electron-doped hydride compounds at high pressure

Shunwei Yao,[1] Qilin Song,[1] Wenjing Hu,[1] Dan Wang,[1] Lin Peng,[1,*] Tingting Shi,[2] Jing Chen,[1] Xiaolin Liu,[1] Jia Lin,[1,†] and Xianfeng Chen[3,4]

[1]*Department of Physics, Shanghai University of Electric Power, Shanghai 200090, China*

[2]*Department of Physics, Jinan University, Guangzhou 510632, China*

[3]*State Key Laboratory of Advanced Optical Communication Systems and Networks, School of Physics and Astronomy, Shanghai Jiao Tong University, Shanghai 200240, China*

[4]*Collaborative Innovation Center of Light Manipulation and Applications, Shandong Normal University, Jinan 250358, China*

(Received 26 October 2021; accepted 23 February 2022; published 10 March 2022)

The recent theoretical discovery of the predicted high-temperature superconductivity (superconducting transition temperature $T_c \sim 351$ K at 300 GPa) in clathrate Li_2MgH_{16} is an important advance toward room-temperature superconductors. Here we use first-principle approaches to identify a new ternary hydride of clathrate structure of $Fd\bar{3}m$-Rb_2MgH_{16} by Rb-doped MgH_{16} at 300 GPa. We first verified the thermal and dynamic stability for the $Fd\bar{3}m$-Rb_2MgH_{16} through the formation enthalpy and phonon calculations, respectively. Next, we showcased that $Fd\bar{3}m$-Rb_2MgH_{16} has two Fermi surface (FS) sheets, which are both dominated by the H2 *s* orbital. Using the Eliashberg formalism, the T_c of $Fd\bar{3}m$-Rb_2MgH_{16} was calculated to be 130 K at 300 GPa. Furthermore, the calculations of the electronic, phonon, and superconducting properties reveal that $Fd\bar{3}m$-Li_2MgH_{16} has four FS sheets with mixed H1 *s* and H2 *s* orbital character and reaches the T_c of 352 K at 300 GPa. Compared with $Fd\bar{3}m$-Rb_2MgH_{16}, $Fd\bar{3}m$-Li_2MgH_{16} produces high-frequency phonon softening, leading to the enhancement of T_c. Moreover, it is demonstrated that Rb substitution for Li produces the reduction of contribution of H orbitals to the FS sheets and the decrease in FS sheets in number, which tend to decrease the electron-phonon coupling strength and T_c. Our observed FS sheets and their associated superconducting gap will provide key insights into the understanding of the superconductivity mechanism in these and related systems.

DOI: 10.1103/PhysRevMaterials.6.034801

I. INTRODUCTION

An important approach of looking for high-temperature superconductors in hydrogen-rich hydrides has been proposed due to the discovery of a superconducting transition temperature (T_c) of 8 K in Th_4H_{15} at ambient pressure in 1970 [1]. However, this strategy was not widely accepted until Ashcroft proposed that hydrogen-rich compounds containing main group elements might exhibit superconductivity at lower pressures compared with metallic hydrogen as the hydrogen in these hydrogen-rich compounds may be considered "chemically precompressed" [2]. Following this idea, it is necessary to carry out extensive theoretical and experimental studies to find high-temperature superconductors in hydride compounds [3–8].

Recently, hydrogen-rich materials as the main candidate for high-T_c superconductors have attracted more and more attention because the theoretical studies predicted sodalitelike clathrate LaH_{10} to have a T_c of ~280 K at 200 GPa [9,10]. Some subsequent experiments confirmed that the theoretically predicted, the synthesized structure of LaH_{10} was measured to have a high superconductivities of $T_c \sim 250$K at pressures above 170 GPa, setting a record high T_c for superconductors [11–13]. Another key advance is that the theoretically predicted cubic SH_3s are confirmed by experimental studies to have high-temperature superconductivity with a T_c of ~204 K at 200 GPa [14–17]. In these observations, the theoretical studies are always meaningful for material science innovation to design novel superconducting materials [18,19].

Nearly all binary hydrides have been investigated by structure searching simulations [4,5,7], among which, simple hydrides with the highest predicted T_c are MgH_6 (271 K at 300 GPa) [20], CaH_6 (235 K at 150 GPa) [21], and YH_6 (264 K at 120 GPa) [22]. These studies stimulate more efforts to look for high-temperature superconductors in binary hydrides as well as ternary hydrides [23–25]. Encouragingly, an experimental work has measured the C-S-H system to have room-temperature superconductivities with a high T_c of 290 K at 270 GPa [26]. Although structural information is unknown of this ternary system, this result still clearly indicates that it is a feasible way of looking for high-temperature superconductors in ternary hydrogen-rich compounds. Very recently, a metastable phase Li_2MgH_{16} is predicted with a T_c of 351 K at 300 GPa via Li-doped MgH_{16}. Li acts as a donor, which dopes extra electrons into the system to enhance the superconductivity of the MgH_{16} system ($T_c \sim 73$ K at 300 GPa) [27]. This result indicates that metal doping is an effective way to design new high-T_c superconductors in hydrogen-rich hydrides. This

*Corresponding author: plpeng@shiep.edu.cn
†jlin@shiep.edu.cn

is reminiscent of Rb having a low electronegativity among the alkali metals. It is natural to wonder if the extra electrons introduced via Rb-doped MgH_{16} may effectively tune the crystal structures and improve the superconductivity for the MgH_{16} system [21].

In this paper, we identify a new ternary hydride of $Fd\bar{3}m$-Rb_2MgH_{16} by Rb-doped MgH_{16} at 300 GPa based on the density functional theory [28]. First of all, the thermal and dynamical stabilities were verified by the formation enthalpy and phonon calculations. Next, through systematic first-principles calculations, we demonstrated that $Fd\bar{3}m$-Rb_2MgH_{16} has two Fermi surface (FS) sheets, which are both dominated by the H2 *s* orbital. The superconductivity calculations show that the T_c of $Fd\bar{3}m$-Rb_2MgH_{16} reaches 130 K at 300 GPa. We find, however, that Rb substitution for Li generates a substantial change in structure and electronic properties in this system, leading to the reduction of T_c of $Fd\bar{3}m$-Rb_2MgH_{16}, compared with Li_2MgH_{16}. These studies emphasize the importance of the chemical tuning structural stability and superconductivity via metal doping, which provide a new angle for designing ternary hydride high-T_c superconductors.

II. METHOD

The Vienna *ab initio* simulation package (VASP) was used to calculate structure optimizations, enthalpies, and electronic properties [29]. The exchange correlation functional was parameterized by the Perdew-Burke-Ernzerhof (PBE) model to describe the electron interactions, and the projector augmented wave (PAW) method was chosen to describe electro-ion interactions [30,31]. The Rb $4s^24p^65s^1$ and Li $1s^22s^12p^0$ and Mg $3s^23p^0$ and H $1s^1$ orbitals were included as valence electrons. We set the threshold value for the forces of atomic positions relaxation with 1 meV/Å.

To illustrate the dynamical stability of A_2MgH_{16} (A = Li, Na, K, Rb, and Cs), based on density functional perturbation theory (DFPT), the dispersion calculation was performed using the educible set of a regular $4 \times 4 \times 4$ q-point meshes with a kinetic-energy cutoff of 220 Ry, and the Methfessel-Paxton smearing width of 0.03 Ry was used. The QUANTUM ESPRESSO code was used in our DFPT calculations [32]. Then, the superconducting properties of Rb_2MgH_{16} and Li_2MgH_{16} were calculated by solving the Migdal-Eliashberg formalism using the EPW code [33–35]. Recently, this method was used to study the superconductivity of crystal structure and the high anisotropy of FSs [27,36–39]. The electronic wave functions required for the Wannier interpolation [40,41] within EPW were calculated on uniform and unshifted k-point meshes of size $8 \times 8 \times 8$ for Rb_2MgH_{16} and Li_2MgH_{16}. The optimized norm-conserving Vanderbilt (ONCV) pseudopotentials with the valence electrons of Li $1s^22s^1$, Na $2s^22p^63s^1$, K $3s^23p^64s^1$, Rb $4s^24p^65s^1$, Cs $5s^25p^66s^1$, Mg $2s^22p^63s^2$, and H $1s^1$ orbitals were used [42]. For the Eliashberg equations, we use $20 \times 20 \times 20$ k-point and $20 \times 20 \times 20$ q-point meshes. The frequency cutoff was set to ten times the maximum phonon frequency of the system, and the electrons and phonons smearing in Dirac-δ functions were used with widths of 30 and 0.5 meV, respectively.

The Migdal-Eliashberg equations was solved to study the superconducting properties. The temperature dependence of energy distribution of anisotropic superconducting gap can be estimated along the imaginary axis at the fermion Matsubara frequencies using the anisotropic Migdal-Eliashberg equations,

$$Z_{nk}(i\omega_j) = 1 + \frac{\pi T}{N(\varepsilon_F)\omega_j} \sum_{mk'j'} \frac{\omega_{j'}}{\sqrt{\omega_{j'}^2 + \Delta_{mk'}^2(i\omega_{j'})}} \times \lambda(nk, mk', \omega_j - \omega_{j'})\delta(\varepsilon_{mk'} - \varepsilon_F) \quad (1)$$

$$Z_{nk}(i\omega_j)\Delta_{nk}(i\omega_j) = 1 + \frac{\pi T}{N(\varepsilon_F)\omega_j} \sum_{mk'j'} \frac{\omega_{j'}}{\sqrt{\omega_{j'}^2 + \Delta_{mk'}^2(i\omega_{j'})}} \times [\lambda(nk, mk', \omega_j - \omega_{j'}) - \mu_c^*] \times \delta(\varepsilon_{mk'} - \varepsilon_F), \quad (2)$$

where $Z_{nk}(i\omega_j)$ is the mass renormalization function, $\Delta_{nk}(i\omega_j)$ is the superconducting gap function, $N(\varepsilon_F)$ is the electronic density of states at the Fermi level, μ_c^* is the effective Coulomb pseudopotential parameter, and ω and ε are the vibrational frequency and eigenvalues, respectively. The anisotropic $\lambda(nk, mk', \omega_j - \omega_{j'})$ to be used in the Migdal-Eliashberg equation is given by

$$\lambda(nk, mk', \omega_j - \omega_{j'}) = \int_0^\infty d\Omega \frac{2\Omega}{(\omega_j - \omega_{j'})^2 + \Omega^2} \alpha^2 F(nk, mk', \Omega). \quad (3)$$

Here, α^2F is the isotropic Eliashberg spectral function. As a result, T_c is defined as the temperature at which the leading edge $\Delta_{nk}(i\omega_j)$ superconducting gap disappears.

III. RESULTS AND DISCUSSION

The $Fd\bar{3}m$-Li_2MgH_{16} was predicted to be a potential room-temperature ternary superconductor with a remarkably high estimated T_c of ~351 K at 300 GPa [27]. Similarly, we predicted a new clathrate structure of $Fd\bar{3}m$-Rb_2MgH_{16} by substituting Rb for Li at 300 GPa. The crystal structure search for Rb_2MgH_{16} at 300 GPa was performed by the swarm intelligence-based CALYPSO method [27,43,44]. The structure search reached the convergence after the generation of 2000 structures, and the predicted structure parameters are summarized in Table S1 of the Supplemental Material [45]. Based on the results, we constructure the formation energy convex hull of the Rb-Mg-H system as shown in Fig. S1 of the Supplemental Material [45]. For a new structure, we further calculated the formation enthalpy with the VASP code [29]. The formation enthalpy for Rb_2MgH_{16} can be defined as [46]

$$\Delta H(Rb_2MgH_{16}) = H(Rb_2MgH_{16}) - \frac{2}{19}H(Rb) - \frac{1}{19}H(Mg) - \frac{16}{19}H(H), \quad (4)$$

where $H(Rb_2MgH_{16})$ is the total enthalpy of Rb_2MgH_{16} per atom, and H(Rb), H(Mg), and H(H) are the enthalpy for the pure elements Rb, Mg, and *Cmca*-12-structured solid hydrogen at 300 GPa, $\Delta H(Rb_2MgH_{16})$ is the formation enthalpy of

Rb_2MgH_{16} per atom [47–49]. The H to be used in the enthalpy equation is given by

$$H = E + PV. \tag{5}$$

Here, E is the total energy of compound, P is the value of the pressure, and V is the volume of the compound. The zero-point energy (ZPE) is important to determine the phase stabilities of hydrogen-rich materials. The formation enthalpy ΔH_{zero} with considering ZPE is defined as

$$\Delta H_{zero} = \Delta H + \Delta ZPE, \tag{6}$$

where ΔZPE is the calculated ZPE of Rb_2MgH_{16}. The ΔH_{zero} value of Rb_2MgH_{16} is estimated to be -0.44 eV per atom (Table S2 of the Supplemental Material [45]). The results show that Rb_2MgH_{16} is thermally stable against decomposition into pure elements, but it is the metastable phase with respect to decomposition into the energetically most favorable binary phases. For the metastable phases of $Fd\bar{3}m$-Rb_2MgH_{16}, we also propose a possible synthetic route: $RbH_5 + MgH_4 + H_2 \rightarrow Rb_2MgH_{16}$ with relative formation enthalpy at 300 GPa of -0.025 eV per atom.

The geometry of $Fd\bar{3}m$-Rb_2MgH_{16} is a similar clathrate structure as $Fd\bar{3}m$-Li_2MgH_{16}, which consists of Mg-centered H_{28} cages, Rb-centered H_{18} cages, and no H_2 units (Fig. 1(a) and Fig. S2 of the Supplemental Material [45]). The H atoms have two different positions, which were denoted as H1 and H2, respectively. The H-H bond lengths are 0.97 and 1.08 Å, respectively, which is close to the H-H distance of ∼0.98 Å in atomic metallic hydrogen near 500 GPa [47]. To investigate the bonding nature, the electron localization function (ELF) was calculated as shown in Fig. 2. Here, the H-H bonds possess the feature of covalent bonds, whereas the bonds are ionic between H and Rb/Mg atoms. To analyze the ionicity, the Bader charges were calculated. The result shows that the charges transferring from Rb to H and Mg to H are 0.09 and 1.59 electrons per atom, respectively. It is clearly demonstrated that both Rb and Mg are electron donors in Rb_2MgH_{16}. We have also performed the electronic property calculations of the predicted structure. The electronic band structure and the PDOS are shown in Fig. 1(b). The PDOS reveal that electronic density of states is dominated by H2 atomic electrons at the Fermi level. The band dispersion shows the metallic character at 300 GPa. It is easy to find the two bands (denoted as $n = 1, 2$) crossing the Fermi level. The corresponding FS sheets for the two bands of $n = 1, 2$, which project their electronic states onto H1, H2, Rb, and Mg atoms at each FS sheets as shown in Fig. 1(c). The first FS sheet is topologically similar to a polyhedron centered on the Γ point, which is composed of the H2 s orbital (Fig. S3 of the Supplemental Material [45]). The second FS sheet with the cage shape around the Γ point is also mainly composed of the H2 s orbital (Fig. S3 of the Supplemental Material [45]). Furthermore, the large contribution of the H2 s orbital to the FS sheets results in the emergency of high T_c in Rb_2MgH_{16} as will be demonstrated later.

Before calculating superconducting properties, we calculated the phonon dispersion and projected phonon densities

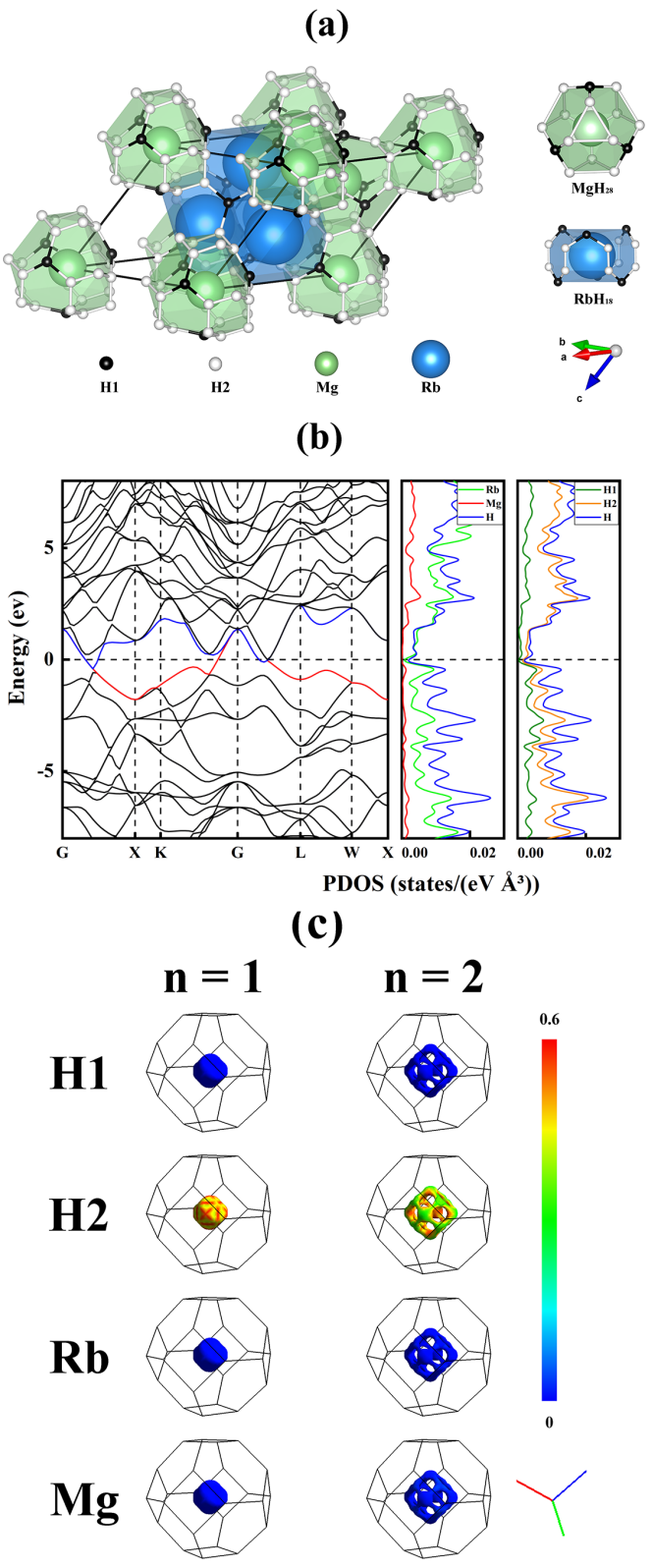

FIG. 1. (a) Predicted crystal structure of $Fd\bar{3}m$-Rb_2MgH_{16} at 300 GPa. (b) Calculated band structure and projected density of states (PDOS) of Rb_2MgH_{16}, and (c) the corresponding FS sheets for the two bands ($n = 1, 2$), which project their electronic states onto H1, H2, Rb, and Mg atoms at each FS sheet.

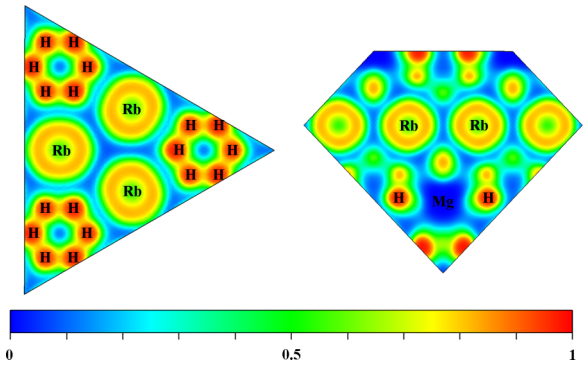

FIG. 2. ELF in (1 1 1) and (1 $\bar{1}$ 4) sections for $Fd\bar{3}m$-Rb_2MgH_{16} at 300 GPa are plotted in the left and right panels, respectively.

of states (PHDOS) as shown in Fig. 3. There is no imaginary frequency in phonon calculation, implying that Rb_2MgH_{16} is dynamically stable. In this case, two regions can be distinguished in the PHDOS: a low-energy region below 500 cm^{-1} and a high-energy region in the range of 500–2500 cm^{-1}. The phonon modes in the low-energy region are associated with the vibration of Rb and Mg atoms. In the high-energy region, the phonon modes with a mixed character are associated with lattice vibration of H1 and H2 atoms, but H2 atoms are dominant, suggesting that the phonon modes of H2 atoms significantly contribute to the electron-phonon coupling (EPC) strength. Specifically, there are no high-frequency vibrations, indicating the absence of molecular H_2 units in Rb_2MgH_{16}. The frequencies of the highest optical phonon modes were calculated to be 2500 cm^{-1}, similar to that of $Fd\bar{3}m$-Li_2MgH_{16} (2400 cm^{-1}) at 300 GPa and the $I4_1$/amd phase of metallic hydrogen (2600 cm^{-1}) at 500 GPa [22,40]. In order to study superconducting properties of Rb_2MgH_{16}, the Eliashberg spectral function and the integrated frequency-dependent EPC strength were calculated (Fig. 3). Electron-coupling calculations for Rb_2MgH_{16} give a λ of 1.90. We can analyze that EPC strength λ increases with ω increases in the region from 0 to 2400 cm^{-1}, suggesting that the phonon modes from all energy regions participate in the increase in λ. The modes (above 500 cm^{-1}) of H1 and H2 atoms contribute approximately 50% of the total EPC strength ($\lambda = 1.90$), and Rb

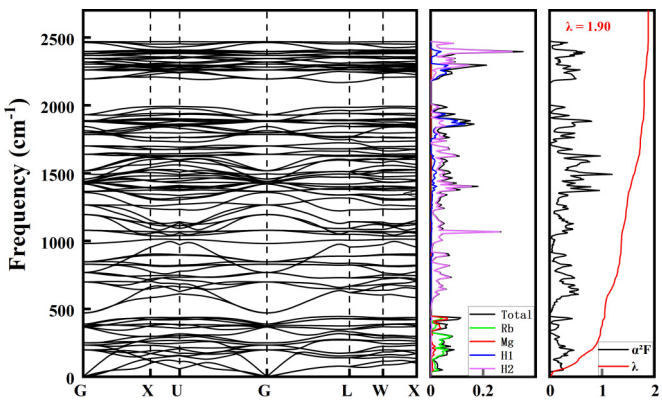

FIG. 3. Phonon spectrum, PHDOS, Eliashberg spectral function, and integrated frequency-dependent EPC strength for Rb_2MgH_{16}.

(below 500 cm^{-1}) and Mg atoms (300–400 cm^{-1}) account for approximately 45% and 5%, respectively. We displayed the normalized distribution of the anisotropic EPC strength on the FS sheets in Fig. S4 of the Supplemental Material [45]. It is noticeable that the distribution of λ on the second FS sheet represents the strong EPC of the $n = 2$ state stemming from the H2 *s* orbital.

In order to illustrate a relationship of the EPC and T_c of Rb_2MgH_{16}, we calculated the temperature dependence of energy distribution of anisotropic superconducting gap Δ. In Figs. 4(a) and S5 of the Supplemental Material [45], T_c is estimated to be 130 K with a typical choice of Coulomb pseudopotential parameter $\mu_c^* = 0.1$ at 300 GPa using the anisotropic Migdal-Eliashberg equations. We found a single superconducting gap with a wide-energy region from 17 to 28 meV at 20 K, which displays a strong anisotropic character. The superconducting gap at 20 K on the two FS sheets of Rb_2MgH_{16} is shown in Fig. 4(b). The distribution of EPC strength and superconducting gap on the two FS sheets are highly similar (Fig. S4 of the Supplemental Material [45]), and the EPC strength and superconducting gap on the two FS sheets are both dominated by the second FS ($n = 2$) sheets. Thus, we can conclude that superconducting gap Δ correlates closely with the EPC strength on the individual FS sheets. In Fig. 4(a), the dashed line represents the calculated superconducting gap by solving the isotropic Migdal-Eliashberg formalism. The superconducting gap of Rb_2MgH_{16} closes at T_c ~130 K. The results demonstrated that the anisotropy of electron-phonon interactions in bands increases T_c by ~14 K, similar to that of metallic hydrogen (~10 K) and LaH_{10} (~19 K) [36,50].

Through the calculations above, we found that the Rb substitution for Li reduces the T_c of Rb_2MgH_{16} compared with $Fd\bar{3}m$-Li_2MgH_{16} (~351 K) at 300 GPa. Thus, we investigated the electronic and superconducting properties of $Fd\bar{3}m$-Li_2MgH_{16} by analyzing FS sheets topology and its associated superconducting gap. The calculated electronic band structure and PDOS of Li_2MgH_{16} are shown in Fig. 5(a). By using the band-PDOS diagram, we found that the electronic density of states of H atoms near the Fermi level in Li_2MgH_{16} is higher than that in Rb_2MgH_{16}, and there are four bands (denoted as $n = 1$–4) crossing the Fermi level. In Fig. 5(b), we display the corresponding FS sheets and the electronic states of the four bands ($n = 1$–4) are projected onto H1, H2, Li, and Mg atoms at each FS sheets. The first FS sheet with mainly mixed H1 *s* and H2 *s* orbital characters is topologically composed of the six small cone shapes surrounding the Γ point (Fig. S6 of the Supplemental Material [45]). The second FS sheet is topologically similar with the complex shape around the Γ point, which is also composed of H1 *s* and H2 *s* orbitals (Fig. S6 of the Supplemental Material [45]). The shape of the third and fourth FS sheets are similar with the dish shape around the *X* point (Fig. S6 of the Supplemental Material [45]). However, these FS sheets have different orbital characters, the third FS sheet is composed of H1 *s* and H2 *s* orbitals, whereas the fourth FS sheet is mostly composed of the H2 *s* orbital.

In order to clarify the superconducting properties of Li_2MgH_{16}, the phonon dispersion, PHDOS, the Eliashberg spectral function, and the integrated frequency-dependent

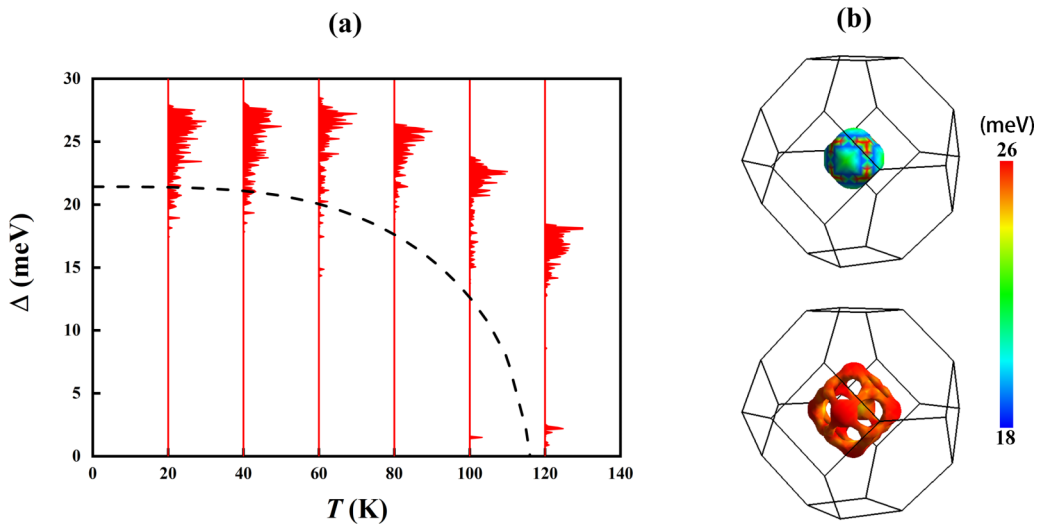

FIG. 4. (a) Calculated temperature dependence of energy distribution of anisotropic superconducting gap of Rb_2MgH_{16}. The dashed line represents the calculated data based on isotropic Migdal-Eliashberg equations. (b) Calculated anisotropic superconducting gap Δ_k at 20 K on different parts of the FS sheets.

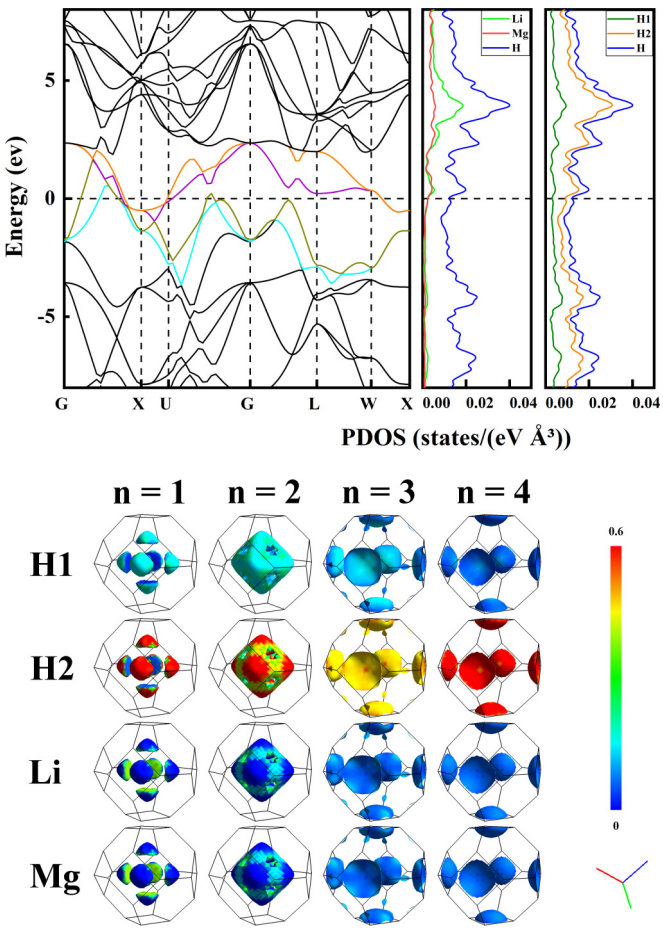

FIG. 5. (a) Calculated band structure and PDOS of Li_2MgH_{16} and (b) the corresponding FS sheets for the four bands ($n = 1$–4), which project their electronic states onto H1, H2, Rb, and Mg atoms at each FS sheet.

EPC strength were calculated (Fig. S7 of the Supplemental Material [45]). The EPC strength (λ) is estimated to be 3.47, which is contributed approximately 35% in the region from 0 to 700 cm^{-1} by Li and Mg atoms. The H1 and H2 atoms account for 65% of the total coupling. For comparison with the Rb_2MgH_{16} system, the frequencies of the highest optical modes of Li_2MgH_{16} are down to 2350 cm^{-1}. The results show that the high-frequency phonon modes produce softening, indicating that the enhancement of λ correlates with the softening of the high-frequency phonon modes. Furthermore, we show the normalized distribution of anisotropic EPC strength on the FS sheets in Fig. S8 of the Supplemental Material [45]. The distribution of λ on the four FS sheets represent the strong EPC of the $n = 1$–4 states stemming from H1 s and H2 s orbitals [Fig. 5(b)]. The results reveal that the larger contribution of H1 s and H2 s orbitals to the FS sheets in Li_2MgH_{16} leads to a considerable enhancement of EPC strength ($\lambda = 3.47$) compared with Rb_2MgH_{16}. It is indicated that the high-temperature superconductivity of hydrides is determined by the contribution of H orbitals to the FS sheets. Thus, we can conclude that λ relates to the orbital characters of the electronic states on the FS sheets. Moreover, the increased number of FS sheets tend to enhance the EPC strength in similar hydride superconductors [36,51]. We subsequently calculated the temperature dependence of superconducting gap Δ as shown in Fig. 6(a). T_c is estimated to be 352 K in $Fd\bar{3}m$-Li_2MgH_{16} at 300 GPa with the Coulomb pseudopotential parameter $\mu_c^* = 0.1$ by solving anisotropic Migdal-Eliashberg equations. For $T < 240$ K, Δ is distributed from 67 to 84 meV. The calculated superconducting gap by solving isotropic Migdal-Eliashberg equations is represented by the dashed line in Fig. 6(a). The superconducting gap of Li_2MgH_{16} closes at $T_c \sim 338$ K, indicating that the anisotropic electron-phonon interactions increase T_c by $\sim$14 K. The single anisotropic superconducting gap of

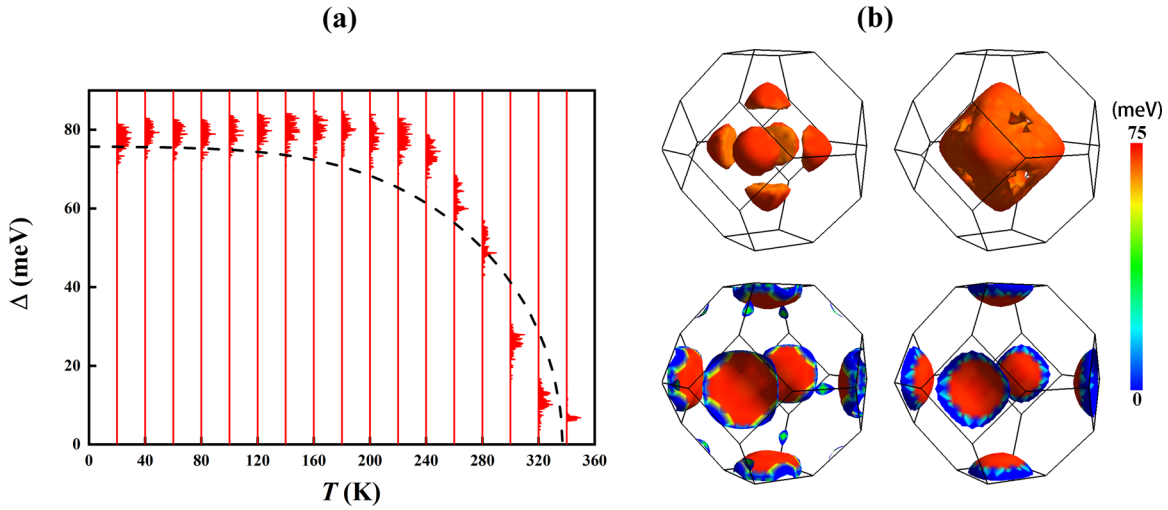

FIG. 6. (a) Calculated temperature dependence of energy distribution of anisotropic superconducting gap of Li_2MgH_{16}. The dashed line represents the calculated data based on isotropic Migdal-Eliashberg equations. (b) Calculated anisotropic superconducting gap Δ_k at 20 K on different parts of the FS sheets.

Li_2MgH_{16} at 20 K on the four FS sheets is shown in Fig. 6(b). It is noticeable that the four FS sheets have different orbital characters. Therefore, based on the results of Δ and λ on the FS sheets, we can conclude that the strong anisotropic is associated with the different contribution of different orbital characters to the FS sheets.

Crystals containing heavier atoms typically host lower characteristic phonon frequencies, which tend to enhance the EPC strength [52]. However, our present calculations demonstrate that heavier Rb substitution for Li generates higher characteristic phonon frequencies. It is demonstrated that $Fd\bar{3}m$-Li_2MgH_{16} produces high-frequency phonon softening, leading to the increase in EPC strength. The EPC channels were reduced also due to the reduced number of FS sheets in Rb_2MgH_{16} compared with $Fd\bar{3}m$-Li_2MgH_{16}, resulting in the decrease in T_c. In addition, we also note that the contribution of H orbitals to the FS sheets is reduced in Rb_2MgH_{16} compared with $Fd\bar{3}m$-Li_2MgH_{16}. Therefore, it is demonstrated that the chemical tuning of the contribution of H orbitals to the FS sheets and the number of FS sheets through the electronic or hole doping is an effective strategic to search hydride high-T_c superconductors [36,53].

In order to evaluate the reliability of our calculation results, we investigated the influence of spin-orbit coupling (SOC) on the bands near the Fermi energy as shown in Fig. S9 of the Supplemental Material [45]. We find that the bands with SOC near the Fermi energy have no obvious changes compared with the bands without SOC (Fig. 1), which show that relativistic effects have little impact on the electronic properties in the Rb_2MgH_{16} system. Therefore, we used the pseudopotential without SOC to analyze the properties of Rb_2MgH_{16}, which could attain the reasonable calculation results. Moreover, we substituted the Li atoms in $Fd\bar{3}m$-Li_2MgH_{16} with Na, K, and Cs at 300 GPa. We find that Na, K, and Cs substitution for Li produces substantial phonon softening in the system (Fig. S10 of the Supplemental Material [45]), which indicated that Na_2MgH_{16}, K_2MgH_{16} and Cs_2MgH_{16} are dynamically instable. The close similarity of the crystal structures A_2MgH_{16} (A = Li, Na, K, Rb, and Cs) allows an explanation of different dynamical stability: The degree of (in)stability of the alkali cation determines the stability of the compounds [54].

IV. CONCLUSION

To summarize, we predicted a ternary hydride of the clathrate structure of $Fd\bar{3}m$-Rb_2MgH_{16} by Rb-doped MgH_{16} at 300 GPa. The formation enthalpy calculations verified that $Fd\bar{3}m$-Rb_2MgH_{16} is a metastable phase compound, and the phonon calculations show that the $Fd\bar{3}m$-Rb_2MgH_{16} is dynamically stable. The first-principles calculations for $Fd\bar{3}m$-Rb_2MgH_{16} have shown that the constituent atoms on the two FS sheets are coupled with the phonon modes in the whole energy regions, indicating that phonon modes have a significant contribution to the EPC. Specifically, we displayed a single anisotropic superconducting gap on the two FS sheets of Rb_2MgH_{16}. It is, thus, revealed that the superconductivity of Rb_2MgH_{16} (T_c ~130 K) is determined by the contribution of H2 s orbitals to the two FS sheets. In addition, the calculations revealed Li_2MgH_{16} has four FS sheets with mixed H1 s and H2 s orbital character and reaches the T_c of 352 K at 300 GPa. Compared with Rb_2MgH_{16}, Li_2MgH_{16} produces high-frequency phonon softening. Moreover, we find that Rb substitution for Li results in the reduction of the EPC channels and contribution of H orbitals to FS sheets, leading to a smaller T_c in Rb_2MgH_{16} compared with Li_2MgH_{16}. Our present findings may be helpful to find more hydrogen-rich high-T_c superconductors in the extended compositional space, thereby identifying the dominant microscopic mechanisms of high-temperature superconductivity in these and related systems.

ACKNOWLEDGMENTS

This work was supported by the National Natural Science Foundation of China (Grants No. 12174246, No. 61875119),

Science and Technology Commission of Shanghai Municipality (Grant No. 21010501300), the Program for Professor of Special Appointment (Eastern Scholar) at Shanghai Institutions of Higher Learning, and Shanghai Rising-Star Program (Grant No. 19QA1404000).

The authors declare no competing financial interest.

[1] C. B. Satterthwaite and I. L. Toepke, Phys. Rev. Lett. **25**, 741 (1970).
[2] N. W. Ashcroft, Phys. Rev. Lett. **92**, 187002 (2004).
[3] C. J. Pickard, I. Errea, and M. I. Eremets, Annu. Rev. Condens. Matter Phys. **11**, 57 (2020).
[4] J. A. Flores-Livas, L. Boeri, A. Sanna, G. Profeta, R. Arita, and M. Eremets, Phys. Rep. **856**, 1 (2020).
[5] T. Bi, N. Zarifi, T. Terpstra, and E. Zurek, *Reference Module in Chemistry, Molecular Sciences and Chemical Engineering* (Elsevier, Amsterdam, 2019).
[6] M. I. McMahon and R. J. Nelmes, Chem. Soc. Rev. **35**, 943 (2006).
[7] H. Wang, X. Li, G. Y. Gao, Y. W. Li, and Y. M. Ma, WIREs Comput. Mol. Sci. **8**, e1330 (2018) .
[8] G. Gao, L. Wang, M. Li, J. Zhang, R. T. Howie, E. Gregoryanz, V. V. Struzhkin, L. Wang, and J. S. Tse, Mater. Today Phys. **21**, 100546 (2021).
[9] H. Liu, Naumov II, R. Hoffmann, N. W. Ashcroft, and R. J. Hemley, Proc. Natl. Acad. Sci. USA. **114**, 6990 (2017).
[10] A. P. Durajski, C. Wang, Y. Li, R. Szczęśniak, and J. H. Cho, Ann. Phys. (Berlin) **533**, 2000518 (2020).
[11] M. Somayazulu, M. Ahart, A. K. Mishra, Z. M. Geballe, M. Baldini, Y. Meng, V. V. Struzhkin, and R. J. Hemley, Phys. Rev. Lett. **122**, 027001 (2019).
[12] Z. M. Geballe, H. Liu, A. K. Mishra, M. Ahart, M. Somayazulu, Y. Meng, M. Baldini, and R. J. Hemley, Angew. Chem. **57**, 688 (2018).
[13] A. P. Drozdov, P. P. Kong, V. S. Minkov, S. P. Besedin, M. A. Kuzovnikov, S. Mozaffari, L. Balicas, F. F. Balakirev, D. E. Graf, V. B. Prakapenka *et al.*, Nature (London) **569**, 528 (2019).
[14] Y. Li, J. Hao, H. Liu, Y. Li, and Y. Ma, J. Chem. Phys. **140**, 174712 (2014).
[15] I. Errea, M. Calandra, C. J. Pickard, J. R. Nelson, R. J. Needs, Y. Li, H. Liu, Y. Zhang, Y. Ma, and F. Mauri, Phys. Rev. Lett. **114**, 157004 (2015).
[16] Y. Li, L. Wang, H. Liu, Y. Zhang, J. Hao, C. J. Pickard, J. R. Nelson, R. J. Needs, W. Li, Y. Huang, I. Errea, M. Calandra, F. Mauri, and Y. Ma, Phys. Rev. B **93**, 020103(R) (2016).
[17] A. P. Drozdov, M. I. Eremets, I. A. Troyan, V. Ksenofontov, and S. I. Shylin, Nature (London) **525**, 73 (2015).
[18] X. Li, Y. Xie, Y. Sun, P. Huang, H. Liu, C. Chen, and Y. Ma, J. Phys. Chem. Lett. **11**, 935 (2020).
[19] P. Zhang, Y. Sun, X. Li, J. Lv, and H. Liu, Phys. Rev. B **102**, 184103 (2020).
[20] X. Feng, J. Zhang, G. Gao, H. Liu, and H. Wang, RSC Adv. **5**, 59292 (2015).
[21] H. Wang, J. S. Tse, K. Tanaka, T. Iitaka, and Y. Ma, Proc. Natl. Acad. Sci. USA. **109**, 6463 (2012).
[22] Y. Li, J. Hao, H. Liu, J. S. Tse, Y. Wang, and Y. Ma, Sci. Rep. **5**, 9948 (2015).
[23] A. P. Durajski and R. Szczesniak, Phys. Chem. Chem. Phys. **23**, 25070 (2021).
[24] M. Du, Z. Zhang, T. Cui, and D. Duan, Phys. Chem. Chem. Phys. **23**, 22779 (2021).
[25] E. F Talantsev, J. Phys.: Condens. Matter **33**, 285601 (2021).
[26] E. Snider, N. Dasenbrock-Gammon, R. McBride, M. Debessai, H. Vindana, K. Vencatasamy, K. V. Lawler, A. Salamat, and R. P. Dias, Nature (London) **586**, 373 (2020).
[27] Y. Sun, J. Lv, Y. Xie, H. Liu, and Y. Ma, Phys. Rev. Lett. **123**, 097001 (2019).
[28] P. Hohenberg, and W. Kohn, Phys. Rev. **136**, B864 (1964); W. Kohn, and L. J. Sham, **140**, A1133 (1965).
[29] G. G. Kresse and J. J. Furthmüller, Phys. Rev. B **54**, 11169 (1996).
[30] G. X. Zhang, A. Tkatchenko, J. Paier, H. Appel, and M. Scheffler, Phys. Rev. Lett. **107**, 245501 (2011).
[31] P. E. Blöchl, Phys. Rev. B **50**, 17953 (1994).
[32] P. Giannozzi, S. Baroni, N. Bonini, M. Calandra, R. Car, C. Cavazzoni, D. Ceresoli, G. L. Chiarotti, M. Cococcioni, I. Dabo *et al.*, J. Phys.: Condens Matter **21**, 395502 (2009).
[33] E. R. Margine and F. Giustino, Phys. Rev. B **87**, 024505 (2013).
[34] J. Noffsinger, F. Giustino, B. D. Malone, C.-H. Park, S. G. Louie, and M. L. Cohen, Comput. Phys. Commun. **181**, 2140 (2010).
[35] S. Ponce, E. R. Margine, C. Verdi, and F. Giustino, Comput. Phys. Commun. **209**, 116 (2016).
[36] C. Wang, S. Yi, and J.-H. Cho, Phys. Rev. B **101**, 104506 (2020).
[37] M. Gao, Q.-Z. Li, X.-W. Yan, and J. Wang, Phys. Rev. B **95**, 024505 (2017).
[38] J.-J. Zheng and E. R. Margine, Phys. Rev. B **95**, 014512 (2017).
[39] L. V. Begunovich, A. V. Kuklin, G. V. Baryshnikov, R. R. Valiev, and H. Agren, Nanoscale **13**, 4799 (2021).
[40] N. Marzari, A. A. Mostofi, J. R. Yates, I. Souza, and D. Vanderbilt, Rev. Mod. Phys. **84**, 1419 (2012).
[41] A. A. Mostofi, J. R. Yates, Y.-S. Lee, I. Souza, D. Vanderbilt, and N. Marzari, Comput. Phys. Commun. **178**, 685 (2008).
[42] D. R. Hamann, Phys. Rev. B **88**, 085117 (2013).
[43] Y. Wang, J. Lv, L. Zhu, and Y. Ma, Comput. Phys. Commun. **183**, 2063 (2012).
[44] Y. Wang, J. Lv, L. Zhu, and Y. Ma, Phys. Rev. B **82**, 094116 (2010).
[45] See Supplemental Material at http://link.aps.org/supplemental/10.1103/PhysRevMaterials.6.034801 for the convex hulls of Rb-Mg-H compounds, the structure of Li_2MgH_{16}, the projected band structure of $Fd\bar{3}m$-Rb_2MgH_{16}, the normalized distribution of the anisotropic EPC on the two FS sheets of Rb_2MgH_{16}, the temperature dependence of energy distribution of anisotropic superconducting gap of Rb_2MgH_{16}, and the projected band structure of $Fd\bar{3}m$-Li_2MgH_{16}. The phonon spectrum, PHDOS, Eliashberg spectral function, and integrated frequency-dependent EPC strength for Li_2MgH_{16}, the normalized distribution of the anisotropic EPC on the two FS sheets of Li_2MgH_{16}, the electronic band structure of

Rb_2MgH_{16} with SOC, phonon spectrum relations, the predicted structural parameters of Rb_2MgH_{16} at 300 GPa, and the calculated energy, enthalpy, and the ZPE value for compounds at 300 GPa.

[46] C. Wolverton and V. Ozoliņš, Phys. Rev. B **73**, 144104 (2006).

[47] J. M. McMahon and D. M. Ceperley, Phys. Rev. Lett. **106**, 165302 (2011).

[48] Y. Ma, A. R. Oganov, and Y. Xie, Phys. Rev. B **78**, 014102 (2008).

[49] H. Olijnyk and W. B. Holzapfel, Phys. Rev. B **31**, 4682 (1985).

[50] P. Cudazzo, G. Profeta, A. Sanna, A. Floris, A. Continenza, S. Massidda, and E. K. U. Gross, Phys. Rev. B **81**, 134506 (2010).

[51] Y. N. Huang, D. Y. Liu, L. J. Zou, and W. E. Pickett, Phys. Rev. B **93**, 195148 (2016).

[52] P. B. Allen and R. C. Dynes, Phys. Rev. B **12**, 905 (1975).

[53] D. C. Lonie, J. Hooper, B. Altintas, and E. Zurek, Phys. Rev. B **87**, 054107 (2013).

[54] J. Kuneš, T. Jeong, and W. E. Pickett, Phys. Rev. B **70**, 174510 (2004).